Manuscript Submitted to JGR Solid Earth

This manuscript is submitted to JGR Solid Earth and is available as a preprint on EarthArxiv.

27 May 2025

Observations of Rayleigh and Love wave Azimuthal Anisotropy Across Alaska

Xiongwei Liu[1], Chuanming Liu[2], and Michael H. Ritzwoller[1]

[1]Department of Physics, University of Colorado Boulder, Boulder, CO, USA.

[2]Institute for Geophysics & Department of Earth and Planetary Sciences, Jackson School of Geosciences, The University of Texas at Austin, Austin, TX, USA.

Corresponding author: Xiongwei Liu, (Xiongwei.Liu@colorado.edu)

†Additional author notes should be indicated with symbols (current addresses, for example).

Key Points:

- Rayleigh wave and Love wave 2ψ and 4ψ azimuthal anisotropy are observed from 10 to 50 s period based on ambient noise data.
- Love wave 2ψ and Rayleigh wave 4ψ with complementary trends in Rayleigh and Love wave amplitudes are caused by Rayleigh-Love coupling.
- The fast axes of various components of anisotropy are related, consistent with expectations for a tilted transversely isotropic medium.

Abstract

Using ambient noise data from 10 s to 50 s period across Alaska, we confirm previous estimates of Rayleigh wave 2ψ azimuthal anisotropy and present the first estimates of Rayleigh wave 4ψ and Love wave 2ψ and 4ψ azimuthal anisotropy, where ψ is the angle of propagation. As in earlier studies, the fast axis orientations of Rayleigh wave 2ψ are mainly parallel to major faults in Alaska at all periods. We also find that on average the fast axis of Love wave 4ψ is rotated 45° relative to Rayleigh wave 2ψ, the fast axis of Rayleigh wave 4ψ aligns with Love wave 2ψ, and the fast axis differences of Rayleigh and Love wave 2ψ range between 0 and 90 degrees with many between 40 to 60 degrees. These observations are consistent with non-elliptical anisotropy with the ellipticity parameters η_K and η_X considerably smaller than 1. Observations of Love wave 2ψ and Rayleigh wave 4ψ reflect strong Rayleigh-Love coupling, which causes the observed complementary trends with period of the amplitudes of Rayleigh and Love wave 2ψ and Rayleigh and Love wave 4ψ. Recent theories of Rayleigh-Love coupling based on a quasi-degenerate theory allow these observations to be understood and to be used in the future to improve models of the elastic tensor in the crust and mantle.

Plain Language Summary

We conduct surface wave ambient noise tomography across Alaska. We found strong azimuthal anisotropy including both Rayleigh wave and Love wave 2ψ and 4ψ azimuthal anisotropy. These signals provide a basis for constructing a more accurate seismic model and are consistent with a newly developed quasi-degenerate theory that incorporates Rayleigh-Love coupling.

1 Introduction

Because surface waves propagate horizontally, surface wave phase speed in anisotropic media depends on the azimuth of propagation ψ. Based on non-degenerate perturbation theory (or Rayleigh's Principle) in which Rayleigh and Love waves interact only weakly, Smith and Dahlen (1973) demonstrated that in a weakly anisotropic medium the azimuthal variation of Rayleigh and Love wave phase and group speeds at angular frequency ω is of the form

$$c(\psi) = c_0[1 + \frac{A_2}{2}\cos(2(\psi - \psi_2)) + \frac{A_4}{2}\cos 4(\psi - \psi_4)] \quad (1)$$

where c_0 is the isotropic speed, ψ is measured clockwise from north, ψ_2 and A_2 are the fast axis and peak-to-peak amplitude for 2ψ, and ψ_4 and A_4 are the fast axis and peak-to-peak amplitude for 4ψ, respectively. They argued that the azimuthal dependence of Rayleigh wave speed will be dominated by the 2ψ term in equation (1) whereas the Love wave speeds will be dominated by the 4ψ term. Montagner and Nataf (1986) presented straightforward integral expressions so that observations of the frequency dependence of the coefficients in equation (1) can be used to invert for depth-dependent components of the elastic tensor. They also argued that fast axes for the 2ψ terms for Rayleigh and Love waves should be out of phase by 90 degrees. The observation of odd-symmetry components (e.g., 1ψ) has been explained by scattering or body-wave interference (Lin & Ritzwoller, 2011; Mauerberger et al., 2020; Zeng et al., 2024).

Based on these studies, focus has been placed on observing and interpreting the modes of anisotropy expected if Rayleigh and Love waves couple only weakly: the 2ψ component of Rayleigh wave anisotropy and the harder to observe 4ψ component of Love wave anisotropy. Many studies have presented and interpreted the 2ψ component of Rayleigh wave anisotropy observed with earthquake data, dating back to the mid-1970s (e.g., Forsyth, 1975; Tanimoto & Anderson, 1985; Montagner and Jobert, 1988; Leveque et al., 1988; Nishimura and Forsyth, 1988, and many others). More recently, these observations have been expanded to include ambient noise observations at higher spatial resolution (e.g., Yao et al., 2010; Lin et al., 2011, and others) and full waveform inversion (e.g., Yuan & Romanowicz,, 2010; Zhu & Tromp 2013, and others). Inversions based on it have been performed to estimate apparent azimuthal anisotropy (Lin et al., 2011; Zhu et al., 2020) as well as inherent anisotropy represented by the elastic tensor (e.g., Xie et al., 2015; Xie et al., 2017; C. Liu & Ritzwoller 2024). Observations of the 4ψ component of Love wave anisotropy are much more rare (e.g., Montagner & Tanimoto, 1990; Trampert and Woodhouse, 2003; Visser et al., 2008; Ekstrom, 2011; Yuan & Beghein 2014; Russell et al., 2019).

Less effort has been devoted to observing the 2ψ variation of Love wave phase speeds and the 4ψ component of the Rayleigh waves. Nevertheless, several studies have found that fundamental mode surface waves appear to possess both 2ψ and 4ψ variations with azimuth (e.g., Montagner & Tainimoto, 1990; Trampert & Woodhouse, 2003; Visser et al., 2008; Polat et al., 2012; Russell et al., 2019). Most of these studies have been performed on a global scale, whereas the local area study of Russell et al. (2019) was performed in a narrow period range (5 - 7.5 s). Recently, X. Liu and Ritzwoller (2025) show theoretically based on a quasi-degenerate theory that Love wave 2ψ and Rayleigh wave 4ψ anisotropy, which are unexpected based on non-degnerate perturbation theory, are expected when Rayleigh-Love coupling is strong and discuss the nature of the anisotropy that will produce such coupling.

In this study, we use data from the USArray Transportable Array (TA) and regional networks across Alaska (**Fig. 1**) to investigate surface wave anisotropy. Other studies have investigated surface wave anisotropy across Alaska before this study, but have focused on Rayleigh wave 2ψ (e.g., Wang & Tape, 2014; Feng et al., 2020; Liu et al., 2022; C. Liu et al., 2024; Liu et al., 2025). We focus on investigating the existence and nature of anisotropy previously not considered, which includes Love wave 4ψ and anisotropy previously considered to be unexpected: Love wave 2ψ and Rayleigh wave 4ψ anisotropy.

We ask four principal questions for Alaska. (1) Are the expected components of azimuthal anisotropy (Rayleigh wave 2ψ and Love wave 4ψ) observed? (2) Are the unexpected components of azimuthal anisotropy (Love wave 2ψ and Rayleigh wave 4ψ) observed? (3) Are the fast directions of some of these observables related; in particular are the fast axes for the 2ψ components of Rayleigh and Love waves rotated by 90 degrees relative to each other? (4) Do the amplitudes of Rayleigh and Love wave azimuthal anisotropy vary as a function of period consistent with the existence of Rayleigh-Love coupling? We focus on a discussion of the observations. A discussion of their meaning for earth structure will be the subject of a later contribution.

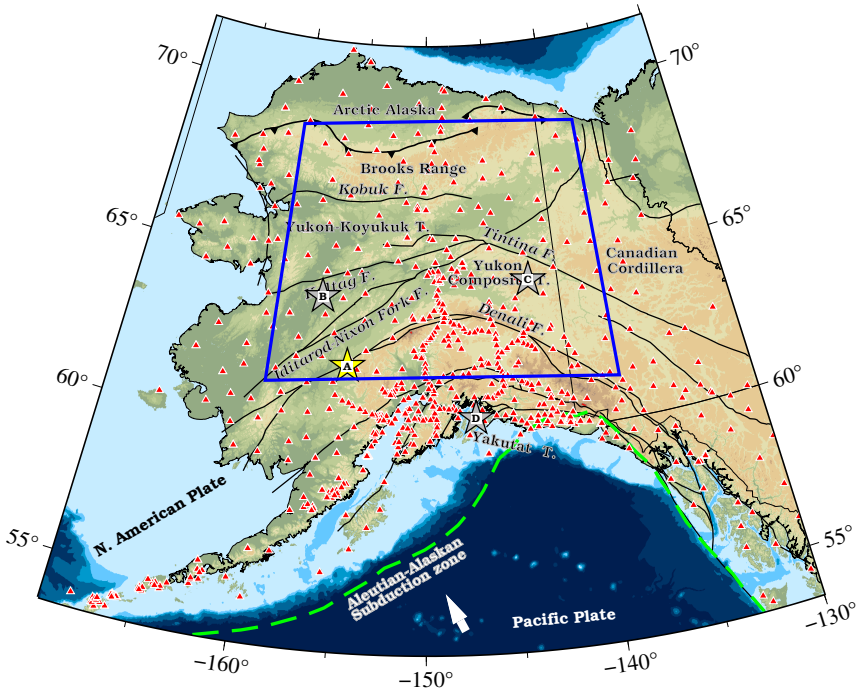

Figure 1. Seismic stations used in the study are shown with red triangles, the yellow star is Point A referred to in **Figure 2**, the gray stars are Point B, C, and D referred to in **Figure 6**, and the blue rectangle is the region used to compute the average amplitude of anisotropy in **Figure 4**. Black lines are major faults.

2 Data and Methods

We use the ambient noise database constructed by Liu et al. (2022), including Rayleigh and Love waves from 10 to 50 s, as input for the tomography and subsequent analysis. This database is based on both traditional two-station ambient noise interferometry (Bensen et al., 2007) and the more recently developed three-station interferometry method (Zhang et al., 2020, 2021). The tomography and observational methods are discussed in section S1 of Supplementary Materials and methods to estimate uncertainty are discussed in section S4. These methods are similar to those applied by Liu et al. (2022), but here we use 36 azimuthal bins rather than 18.

Examples of measurements of the azimuthal variation of Rayleigh and Love wave phase speed at periods of 20 s and 40 s for a location in western Alaska near the Denali fault (Point A of **Figure 1**) are shown in **Figure 2**. At 20 s period, anisotropy is similar to what is expected in the absence of Rayleigh-Love coupling: the Rayleigh wave mainly displays 2ψ anisotropy (**Figure 2a)** and the Love wave mainly 4ψ anisotropy (**Figure 2c)**. However, at longer periods (e.g., 40 s), which are more sensitive to the mantle, the Rayleigh wave mainly shows 4ψ anisotropy (**Figure 2b**) and the Love wave mainly 2ψ anisotropy (**Figure 2d**). This result is an example of the effect of Rayleigh-Love coupling through anisotropy as discussed by X. Liu and Ritzwoller (2025).

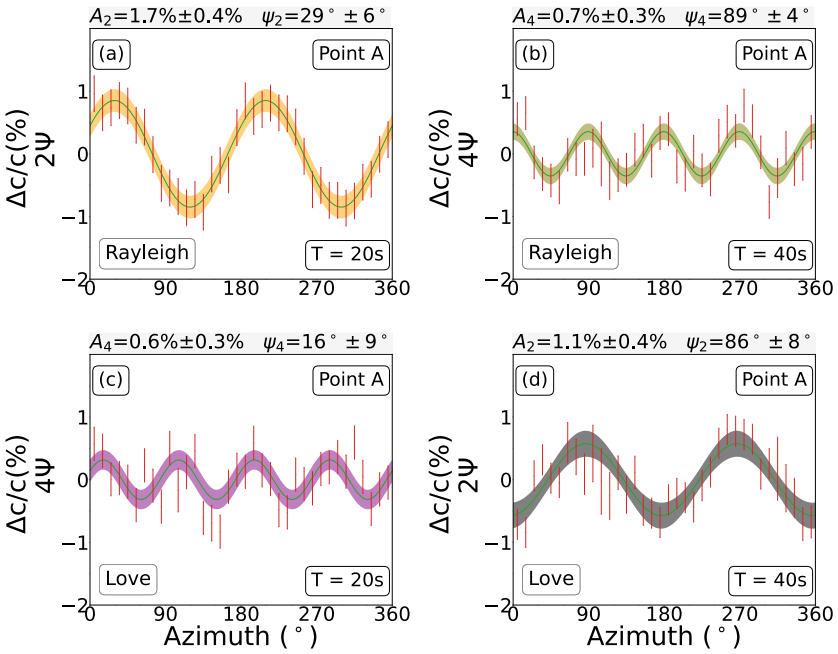

Figure 2. Examples of measurements of Rayleigh and Love anisotropy in western Alaska near the Denali fault, Location A in **Figure 1**. The left column is at 20 s period, the right column is at 40 s, the top row is for Rayleigh waves, and the bottom row is for Love waves. The red bars are the 2ψ or 4ψ components of observations, whichever is dominant, displaying one standard-deviation of the mean in each of 36 azimuthal bins. The estimated amplitude and fast axis of the dominant component of anisotropy are shown at the top of each panel. Each shaded corridor

represents the one standard deviation uncertainty in the estimated phase speed. More complete observations at Point A are shown in **Figures S1-S5**.

3 Results and Discussion

Our results for azimuthal anisotropy are summarized in **Figure 3** at two different periods, one that is mainly sensitive to the crust (20 s) and the other that is principally sensitive to the uppermost mantle (40 s). Expected anisotropy (Rayleigh wave 2ψ and Love wave 4ψ) is presented in the first two rows and unexpected anisotropy (Love wave 2ψ and Rayleigh wave 4ψ) appears in the bottom two rows. Results at other periods are also shown in the Supplementary Materials (**Figure S6**). Maps of the uncertainty in the isotropic phase speed, fast axis orientations, amplitude, and the amplitude of each component of anisotropy normalized by its uncertainy are shown in the Supplementary Materials (**Figures S9-S22**). Here, by 'amplitude' we mean the peak-to-peak amplitude (A_2 and A_4 in equation (1)). For a general anisotropic medium with 21 independent elastic components, the fast axes of different signals (e.g., Rayleigh wave 2ψ, Love wave 2ψ, etc) can have any relationship because they are determined by different independent elastic parameters (X. Liu & Ritzwoller, 2025). However, in a tilted transversely isotropic (TTI) medium the fast axes for different signals may have a specific relationship. We focus on discussing observational results in light of these expectations for a TTI medium.

3.1 Expected anisotropy: Rayleigh wave 2ψ and Love wave 4ψ

"Expected anisotropy" dominates when Rayleigh-Love coupling is weak. The expected anisotropy for Rayleigh waves and Love waves closely mirrors the behavior of SV and SH waves, which display 2ψ and 4ψ, respectively, in the absence of SV-SH coupling (Backus, 1965). Rayleigh wave 2ψ anisotropy has been observed in many studies but Love wave 4ψ has presented a more significant observational challenge. Here, we first discuss these expected signals across Alaska, summarized in **Figure 3a-d** at two periods and **Figure S6** at other periods. We address questions #1 and #3 that motivate this study, notably whether Rayleigh wave 2ψ and

Love wave 4ψ anisotropy are observed across Alaska and if the fast axis orientations of these two components are related.

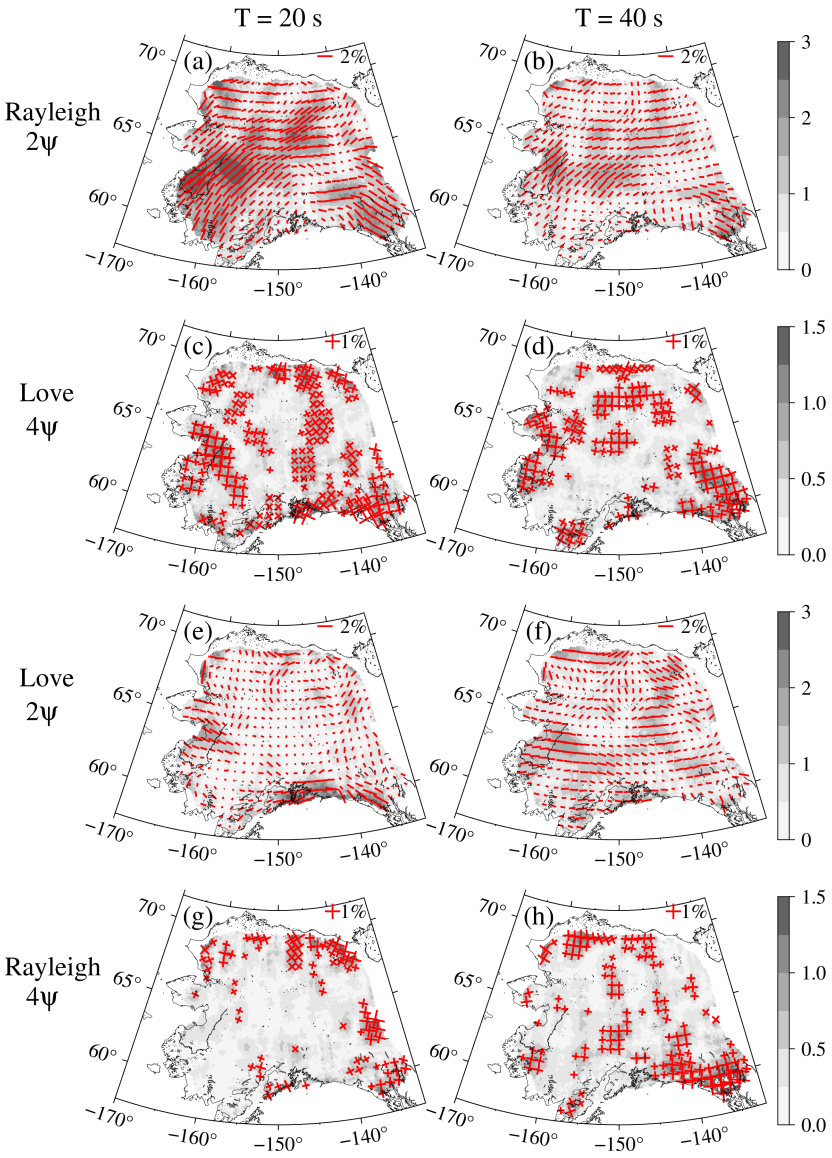

Figure 3. The amplitude and fast axis of Rayleigh (rows 1 and 4) and Love (rows 2 and 3) wave 2ψ and 4ψ azimuthal anisotropy at periods of 20 s (left column) and 40 s (right column). The red bars indicate the fast axis for 2ψ or fast axes for 4ψ, with length proportional to amplitude as shown in each panel. The background grey-shade is the amplitude of the specified component of anisotropy, with units of percent of isotropic phase speed at each location. To reduce clutter, red

crosses are shown for 4ψ anisotropy only when the amplitude is larger than 0.5%, which are the major signals.

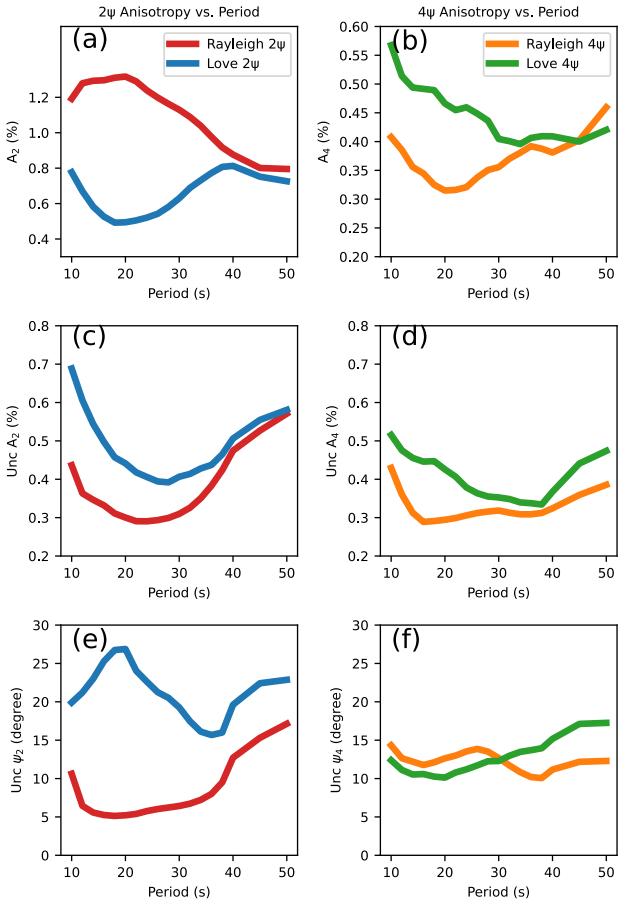

Figure 4. (a)-(b) Spatial average of the amplitude of Rayleigh and Love wave 2ψ and 4ψ compenents of anisotropy, computed within the blue rectangular box shown in **Figure 1** where amplitudes are most reliable. (c)-(f) Uncertainty in the amplitude and fast azimuth orientations of the 2ψ and 4ψ components also computed in the blue box but with an amplitude cutoff: the uncertainty is computed only where the amplitude exceeds the spatial average.

3.1.1 Rayleigh wave 2ψ

After simultaneously resolving the 2ψ and 4ψ components for the Rayleigh wave, our Rayleigh wave 2ψ results (**Fig. 3a,b**) remain very similar to those of Liu et al. (2022). The average amplitude of Rayleigh wave 2ψ (**Figure 4a**) diminishes with period from about 1.3% near 20 s period to about 0.8% at 40s and longer periods. This reduction of amplitude with period is shown for point A in **Figures S1-S5** and it is also visually apparent in **Figure 3a,b**. In contrast, the average uncertainty (**Fig. 4c**) typically grows with period from about 0.3-0.4% at shorter periods

to about 0.5% at 40 s and above. The uncertainties, therefore, are well below the average amplitudes at all periods (**Figure S13**).

The fast axis of Rayleigh wave 2ψ mainly parallels major faults, which suggests that the potential cause of this strong anisotropy is fractures and cracks in the crust (e.g., Feng et al., 2020). This relatively simple fault-parallel pattern plays an important role in the comparison of Rayleigh wave to Love wave azimuthal anisotropy later in section 3.2. The uncertainty in the fast axis direction for Rayleigh wave 2ψ increases with period as the amplitude decreases, with an average of about 5 degrees at 20 s period and 15 degrees at 50 s period.

3.1.2 Love wave 4ψ

A principal novelty of this study is the clear observation of Love wave 4ψ anisotropy over large parts of Alaska (**Figure3c,d**), for example Point A highlighted in **Figure 2** as well as **Figures S1-S5**. Unlike 2ψ, which has two fast directions (a single bar), 4ψ exhibits four fast directions (two bars). As shown in **Figure 4a,b**, the amplitude of Love wave 4ψ is smaller than the Rayleigh wave 2ψ at all periods. Like Rayleigh 2ψ, it diminishes with period but more weakly, from an average of about 0.5% at shorter periods to 0.4% at longer periods. The smaller amplitude of the Love wave 4ψ, particularly at longer periods, poses a challenge to its observation, in addition to the greater azimuthal resolution needed to observe it reliably. The average uncertainty (**Fig. 4d**) is relatively flat with period, averaging between 0.4-0.5%. The average amplitude of the Love wave 4ψ lies closer to but above the uncertainty level on average. The uncertainty normalized amplitude across Alaska is in the supplementary material (**Figure S16**).

Largely due to limitations in azimuthal resolution, previous studies have not discussed the fast axis of Love wave 4ψ or its comparison to Rayleigh wave 2ψ. The uncertainty of the fast axis orientaitons for Love wave 4ψ grows sightly with period from about 10 degrees to 15 degrees (**Figure 4f**) as its average amplitude decreases (**Figure 4b**).

Figure 5a presents the difference between the fast axes of Love wave 4ψ (**Figure 3c,d**) at 20 s period and Rayleigh wave 2ψ (**Figure 3a,b**) at 14 s period, and **Figure 5c** summarizes this difference across Alaska with a histogram. These periods are chosen so that the sensitivity kernels with depth are relatively similar, both being confined to the crust. We find that the mode of the difference is about 45° (**Figure 4c**). **Figure S7** presents another example histogram but for different periods (14 s for Rayleigh, 10 s for Love), which illustrates the fast axis differences accumulating near 45 degrees even more clearly. As discussed by X. Liu and Ritzwoller (2025), observation of a near 45° fast axis difference indicates that the elastic tensor for a TI medium is tilted and the ellipticity parameter $\eta_X < 1$ in the crust or at least in the upper crust. η_X = 4L/(A+C-2F), where A, C, L, and F are inherent Love moduli, and $\eta_X \approx \eta_K$ of Kawakatsu (2016). Exceptions (red colors in **Figure 5a**) lie near the northern and southern boundaries or where the amplitude of 4ψ is small. Locations where we do not observe the 45° difference is often associated with larger measurement uncertainty (e.g., **Figure S14a**). However, there are some regions where Rayleigh wave 2ψ and Love wave 4ψ are quasi-parallel to each other, both with large amplitudes, indicating that the ellipticity parameter $\eta_X > 1$. An example is Location A in western Alaska, with data shown in **Figures 2** and **S1-S5.** Further discussion of the ellipticity

parameter, such as its application in receiver function anisotropy (e.g., Schulte-Pelkum et al., 2020, 2023), is beyond the scope of this paper.

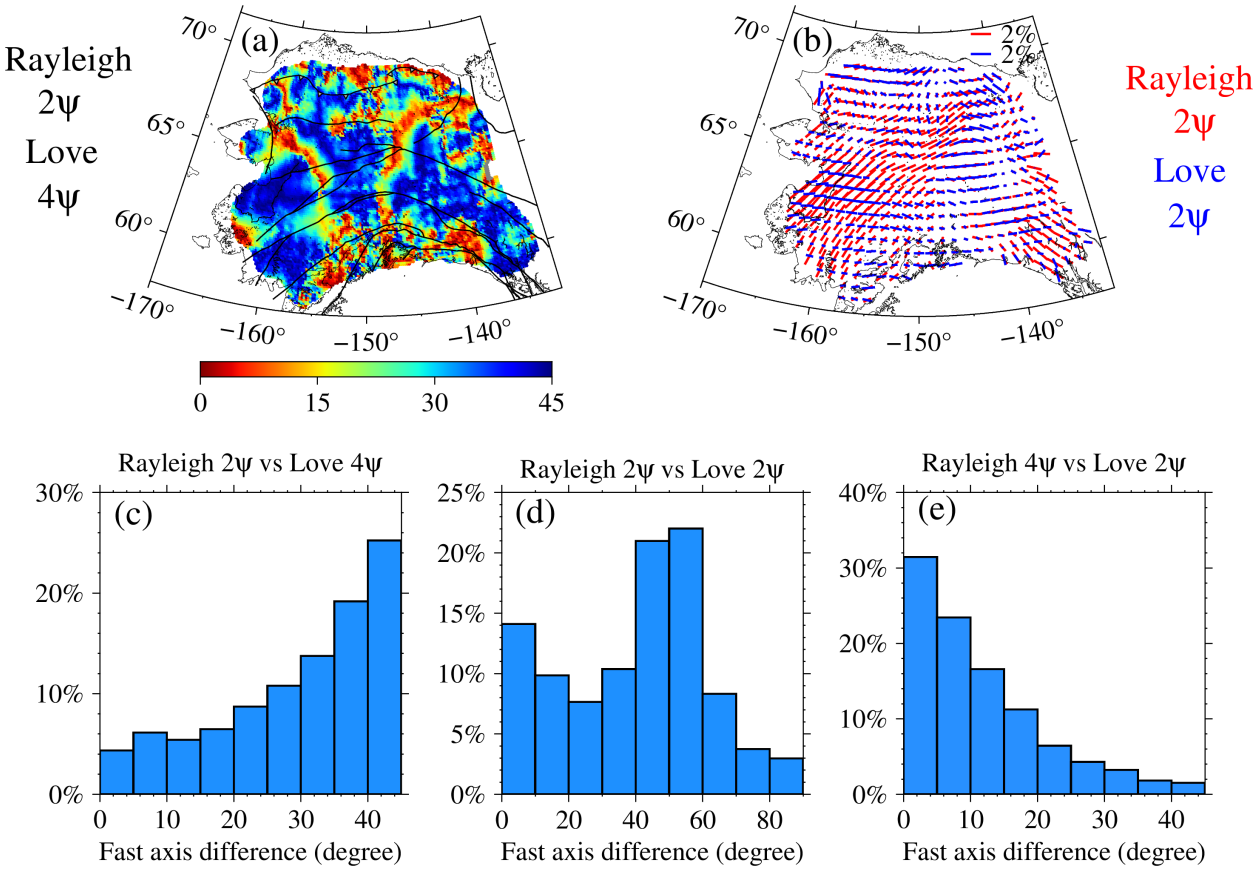

Figure 5. Comparison of fast axes observations. Histograms are computed where the amplitude of the 2ψ component is greater than 0.5%, the amplitude of the 4ψ component is greater than 0.3%, the fast axis uncertainty of the 2ψ component is less than 20 degress, and the fast axis uncertainty of the 4ψ component is less than 15 degress. (a),(c) Comparison is between Rayleigh wave 2ψ at 14 s period and Love wave 4ψ at 20 s period. (b),(d) Comparison is between Rayleigh wave 2ψ at 20 s period and Love wave 2ψ at 40 s period. (e) Comparison is between the Rayleigh wave 4ψ at 45 s period and Love wave 2ψ at 40 s period.

3.2 Unexpected anisotropy: Love wave 2ψ and Rayleigh wave 4ψ

As shown in **Figures 2** and **3**, in addition to the expected anisotropy, at some places and certain periods we observe Love wave 2ψ and Rayleigh wave 4ψ anisotropy, which are unexpected without Rayleigh-Love coupling. Here, we discuss the observation of those unexpected signals across Alaska, which are more prominent at the mantle-sensitive longer periods but also observed at the crust-sensitive shorter periods (e.g. **Figure 6f**). We address questions #2, #3, and #4 that motivate this study, notably whether Rayleigh wave 4ψ and Love wave 2ψ anisotropy are observed across Alaska, if the fast axis orientations of Love wave 2ψ

and Rayleigh wave 2ψ and 4ψ anisotropy are related, and whether the amplitudes of Rayleigh and Love wave anisotropy vary with period consistent with Rayleigh-Love coupling.

3.2.1 Love wave 2ψ

The principal result of this study is the observation of Love wave 2ψ anisotropy, depicted in **Figure 3e,f** and **S6g-i.** The amplitude of this signal on average grows with period from about 0.5% at 20 s period to 0.8% at 40 s period (**Figure 4a)**. The uncertainty (**Fig. 4c**) varies with period, but averages between 0.4-0.6%, so the signal is typically larger than the uncertainty at most points. The uncertainty normalized amplitude across Alaska is shown the supplementary material (**Figure S19**).

Figures 4a and **3a,b,e,f** show that the amplitude of Love wave 2ψ varies with period approximately opposite from Rayleigh wave 2ψ. A detailed local comparison of the amplitudes of Love and Rayleigh wave 2ψ is shown in **Figure 6** for three points in Alaska (Points B, C, and D identified in **Figure 1**). These three points exemplify the spatially averaged statistics presented in **Figure** 4a, that the Love wave 2ψ amplitude increases and the Rayleigh wave 2ψ amplitude decreases with period (**Figure 6**b,d,f) which we infer to result of Rayleigh-Love coupling. For Points B and C, Rayleigh-Love coupling is mainly caused by anisotropy in the mantle. For Point D, when the isotropic phase speed difference minimizes between 20 and 30 s period (**Figure 6**e), the amplitude of Rayleigh wave 2ψ decreases rapidly while the amplitude of Love wave 2ψ increases instead (**Figure 6**f). X. Liu and Ritzwoller (2025) discuss that this is the hallmark of Rayleigh-Love coupling, where the energy of the Rayleigh wave, which is strong at shorter periods, is transmitted to the Love wave through anisotropy coupling at the longer periods. The phase speeds of the Rayleigh and Love waves at Point D are similar enough between 20 and 30 s period (**Figure 6e**) that a small inherent anisotropy around 4% ~ 6% in the crust can cause strong Rayleigh-Love coupling and the large observed amplitude of Love wave 2ψ (**Figure 6f**). Details about the inversion for the depth varying elastic-tensor at these points will be presented in a later contribution.

These points are examples of common observations across Alaska (**Figure 4**a). For some regions in Alaska, the increase of Love wave 2ψ amplitude is not accompanied with a decrease of Rayleigh wave 2ψ amplitude and they may both increase with period. This may also result from

Rayleigh-Love coupling as explained in X. Liu & Ritzwoller (2025). Nevertheless, we find that on average their amplitudes are complementary across Alaska (**Figure** 4a).

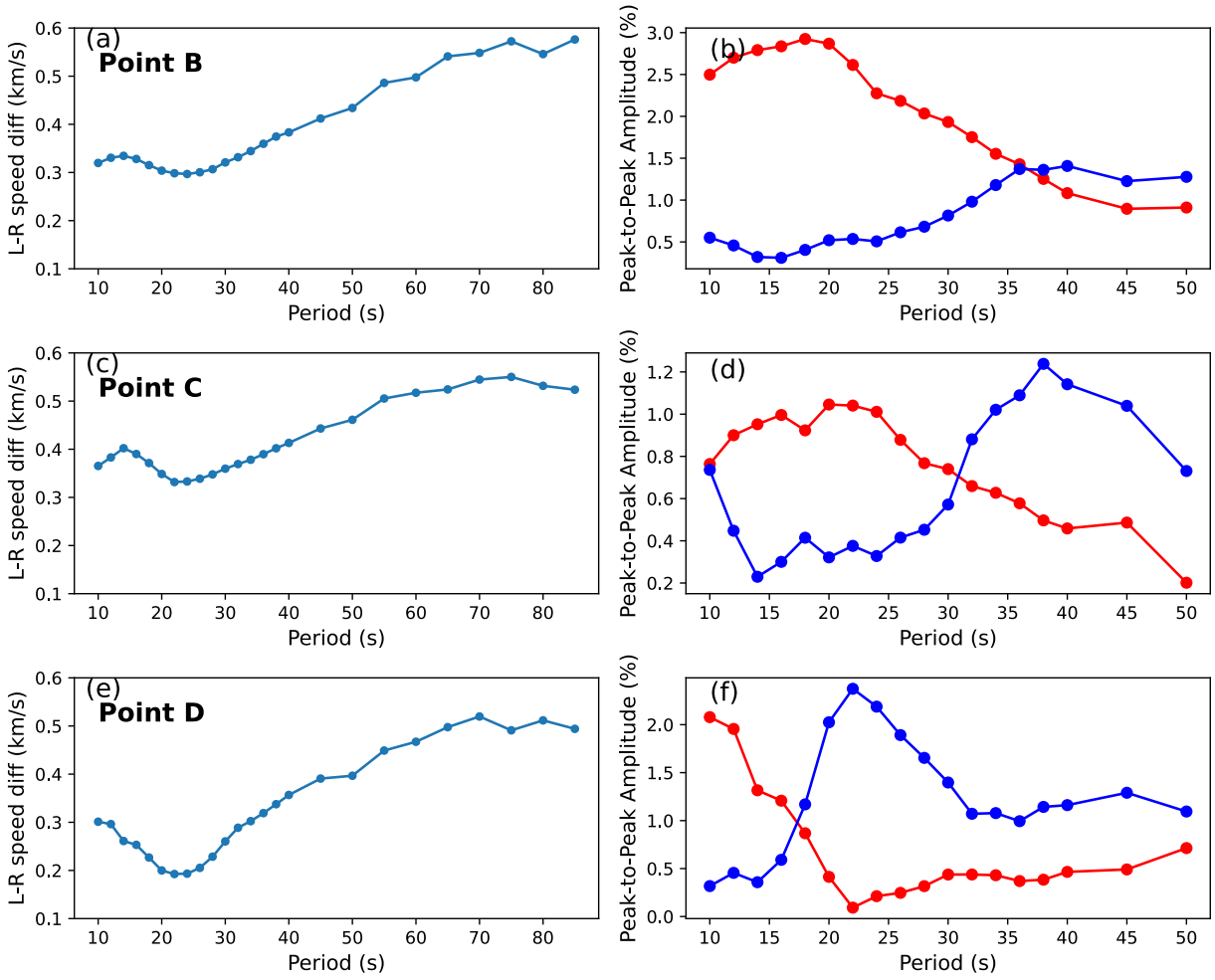

Figure 6. Observational examples of the effect of Rayleigh-Love coupling at three points identified in Figure 1: Point B (first row), Point C (second row), and Point D (third row). (a),(c),(e) The phase speed difference between the Rayleigh wave and Love wave at periods of 10 s – 85 s. (b),(d),(f) The Rayleigh wave 2ψ amplitude (red lines) and the Love wave 2ψ amplitude (blue lines) from 10 s – 50 s period. The dots are our estimated quantities. The isotropic phase speed differences larger than 50 s are based on dispersion measurements from earthquakes taken from Liu et al. (2022).

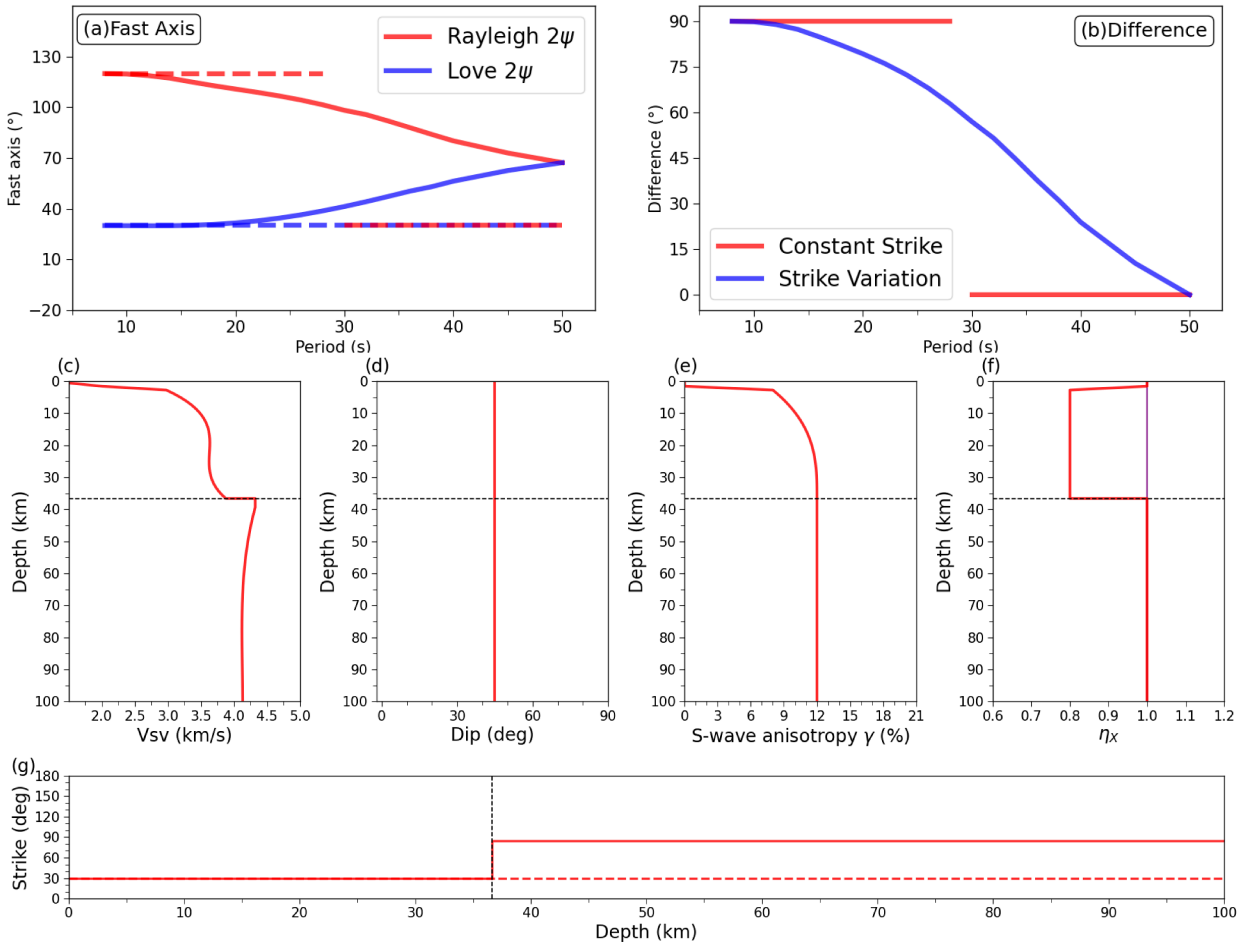

Figure 7. Synthetic test of the effect of strike variation with depth on fast-axes. Two models, aspects of which are shown in (c)-(g), differ only in the strike angle of anisotropy. (a) Fast axes predictions (X. Liu & Ritzwoller, 2025) for Rayleigh 2ψ (red line) and Love 2ψ (blue line) using the two models: solid line (variable stike with depth) and dashed line (constant strike with depth). (b) The fast axis difference between Rayleigh 2ψ and Love 2ψ for the two models of strike variation with depth. (c-g) Aspects of the model used to produce the synthetic results: (c) Vsv =$\sqrt{L/\rho}$, (d) dip angle, (e) radial anisotropy γ = (N-L)/2L, (f) the ellipiticity parameter η_X, and (g) strike angle (solid line constant strike, dashed line variable strike), where L and N are the inherent Love shear moduli. Details about the definitions can be found in Xie et al. (2015) and X. Liu & Ritzwoller (2025).

As with all of the fast axis measurements, the Love wave 2ψ fast axis uncertainty (e.g., **Figure S17**c) is strongly anti-correlated with its amplitude (e.g., **Figure 3f)**; i.e., when the amplitude is high the fast axis uncertainty falls. The fast axis uncertainty for Love wave 2ψ lies between 15 and 25 degrees, which is considerably larger than the uncertainty for the Rayleigh wave 2ψ. This partially reflects the higher noise level on the T-T versus Z-Z components of ambient noise cross-correlations, but also that the Rayleigh 2ψ has a larger amplitude, particularly at shorter periods. Love wave 2ψ fast axis uncertainties are larger than those of Love wave 4ψ because its

azimuthal wavelength is longer by a factor of two (180 degrees versus 90 degrees), so relative uncertainties are about the same.

Figure 5b overplots the Rayleigh and Love wave 2ψ fast axes at 20 s and 40 s period, respectively. We choose 20 s rather than 40 s for comparison because the Rayleigh wave 2ψ amplitude is stronger at 20s period, but its fast axis directions change little between 20 s (**Figure 3**a) and 40 s (**Figure 3**b). In some places in Alaska, particularly in eastern Alaska as **Figure 5b** illustrates, the fast axes are approximately parallel to one another, but more commonly they differ by an angle between 40 and 60 degrees, which occurs across much of western Alaska, which is also reflected in the histogram shown in **Figure 5d**. The relationship between these fast directions is not simple, and we turn to theory to explain the observations.

For very weak Rayleigh-Love coupling, Montagner and Nataf (1986) argued that the 2ψ fast axes for Rayleigh and Love waves should be out of phase by about 90 degrees when they are sensitive to similar depths. Thus, absent strong Rayleigh-Love coupling, the Rayleigh wave 2ψ fast axes would be nearly perpendicular to the Love wave 2ψ fast axes. With strong Rayleigh-Love coupling, however, X. Liu and Ritzwoller (2025) showed that when the strike of anisotropy is constant with depth, the Love wave 2ψ fast axes should align with the strike of anisotropy whereas the Rayleigh 2ψ fast axes could align with the strike or be perpendicular to it. Thus, angle difference between the Rayleigh and Love wave 2ψ fast axes could be either 0 degrees (parallel) or 90 degrees (perpendicular) if the strike of anisotropy is depth-invariant. In fact, we see neither the bimodal distribution (0 or 90 degrees) of fast axis differences predicted if Rayleigh-Love coupling is strong an strike is depth-invariant nor the single 90 degree difference predicted with weak Rayleigh-Love coupling (**Figure 5d**). We believe the reason for this is due to a significant variation in the strike of anisotropy with depth from the the crust to the mantle.

To illustrate the effect of a strike variation with depth we use two synthetic TTI models (**Figure 7**c-g), one with a constrant stike angle with depth and another where the strike angle differs in the crust and mantle (**Figure 7g**). Other aspects of the models are the same, they have a depth-constant dip angle (45°, **Figure 7d**), an almost constant radial anisotropy (12%, **Figure 7e**), but different η_X in the crust and mantle (**Figure 7f**). Both have a strike angle of 30° in the crust, but one continues that strike angle in the mantle and the other has a strike angle of 85° in the mantle. (**Figure 7g**). η_X in the crust differs from 1 which makes the Rayleigh wave 2ψ fast axis perpendicular to the strike in the crust as discussed by Xie et al. (2015).

Figures 7a,b show examples of the fast axes orientations predicted by the theory of X. Liu & Ritzwoller (2025) with stong Rayleigh-Love coupling. With a constant strike angle with depth, the Love wave 2ψ fast axis is the same as the strike direction at all depths. At long periods (>30 s), the Rayleigh wave fast axis aligns with the Love wave fast axis, but at short periods it is perpendicular to it. Thus, with a constant strike angle with depth, the difference between the Rayleigh and Love wave 2ψ fast axes bifurcates to be either 0 or 90 degrees (red line, **Figure 7b**). This is not what we observe, however (**Figure 5d**). Letting the strike angle vary from the crust to mantle, produces a stike angle difference intermediate between 0 and 90 degrees (blue line, **Figure 7b**), similar to our observations. We conclude, therefore, that observed strike angle

differences between Rayleigh wave 2ψ and Love wave 2ψ are evidence for strike variations with depth.

In conclusion, our observation of intermediate fast axes differences (40-60 degrees, **Figure 5b,d**) in western Alaska is diagnostic of a strike variation with depth. We refer to this as the fast axes being "quasi-perpendicular". On average, therefore, Rayleigh and Love wave 2ψ fast axes are approximately quasi-perpendicular across western Alaska and they are approximately parallel across much of eastern Alaska. Thus, strike angles are more likely to vary only subtly with depth across eastern Alaska with stronger variation with depth in western Alaska.

Figure S8 presents another example histogram but for different periods (60 s for Rayleigh, 40 s for Love). This illustrates a stronger bifurcation of the fast axes differences near 0° and 90°, which suggests a more subtle strike variation with depth.

3.2.2 Rayleigh wave 4ψ

Although Trampert & Woodhouse (2003) argued that Rayleigh wave 4ψ should be observable, it has been largely overlooked in studies of anisotropy. We observe Rayleigh wave 4ψ across substantial parts of Alaska at longer periods, as shown in **Figure 3g,h, Figure S6l**, and also in **Figure 2** for an individual location. Rayleigh wave 4ψ is not as strong or ubiquitous as the other components in Alaska, averaging between 0.3-0.45% in amplitude (**Figure 4b**). The uncertainty in the amplitude of Rayleigh wave 4ψ averages between 0.3-0.4% (**Figure 4d**), which is smaller than the observed signal, on average, principally at the long periods. The uncertainty normalized amplitude across Alaska is in the supplementary material (**Figure S22**).

At shorter periods such as 20 s (**Figure 3g**), the amplitude of Rayleigh wave 4ψ is negligible in central Alaska and largest near the periphery of the study region where uncertainties are largest and reliability is suspect. As period increases (**Figure 3h** and **4b**), the amplitude of Rayleigh wave 4ψ becomes comparable to Love wave 4ψ and at 50 s period it is a bit stronger, on average. As illustrated in **Figure 2**, there are locations and periods where the azimuthal variation of the Rayleigh wave is actually dominated by 4ψ. **Figure 4b** and also **Figure 3c,d,g,h** show that the amplitude of Rayleigh wave 4ψ varies with period more or less opposite from Love wave 4ψ. X. Liu and Ritzwoller (2025) say this is what is expected in the presence of Rayleigh-Love coupling, where the amplitude of this component of the Love wave, which is stronger at shorter periods, is transmitted to the Rayleigh wave through anisotropy coupling at the longer periods. Ignoring Rayleigh wave 4ψ, for example, can bias estimates of dip angle and ellipiticy parameters (X. Liu & Ritzwoller, 2025).

Uncertainty in the fast axis direction for Rayleigh wave 4ψ is about 10 degrees, which is similar to the uncertainty for Love wave 4ψ. According to X. Liu & Ritzwoller (2025), the sensitivity kernels of Love wave 2ψ and Rayleigh wave 4ψ are basically the same as they are both mainly determined by the second term in X (equation (45) in X. Liu & Ritzwoller, 2025). Therefore, their fast axes comparison is much more straightforward, compared to comparisons between

Love wave 2ψ and Rayleigh wave 2ψ. We find that Rayleigh wave 4ψ fast axis mainly align with those of Love wave 2ψ (**Figure 5e**).

Although this is beyond the scope of this paper, we note that inversion experiments indicate that strong Rayleigh wave 4ψ at long periods may not be explainable with a TTI mantle, and these observations are more consistent with tilted orthorhombic elastic tensor in the mantle. A tilted orthorhombic medium in the mantle may further complicate the fast axes relationships compared with other signals.

4. Conclusions

Observations of Rayleigh wave and Love wave 2ψ and 4ψ azimuthal anisotropy are presented here across Alaska at periods ranging from 10 s to 50 s based on seismic ambient noise. We discuss the amplitude and fast axis orientations and address the four questions that motivated this study, with the following conclusions:

(1) Both Rayleigh wave 2ψ and Love wave 4ψ are strong across Alaska with the average amplitude of both signals decreasing with period.

(2) Love wave 2ψ and Rayleigh wave 4ψ anisotropy also are observed but with the average amplitudes growing with period. Love wave 2ψ becomes similar in amplitude to Rayleigh wave 2ψ at the longest periods of this study. Rayleigh wave 4ψ is the weakest of the components studied, but is observable at the longer periods.

(3) The fast axes of several components of anisotropy appear to be related. The mode of the distribution of the difference in fast axes between the Rayleigh wave 2ψ and Love wave 4ψ is 45 degrees and between the Love wave 2ψ and Rayleigh wave 4ψ is 0 degrees. The fast axis relationship between Rayleigh and Love wave 2ψ is bimodal (0 and 45-60 degrees), where most differences are in the latter category, which we call quasi-perpendicular. Strike variations of the anisotropic fabric with depth can account for angle differences being substantially different than the expected 0 or 90 degrees for simple seismic models.

(4) We interpret the observations of unexpected anisotopy and the complementary amplitude trends of Rayleigh and Love wave 2ψ as well as Rayleigh and Love wave 4ψ to result from Rayleigh-Love coupling becoming stronger at longer periods as the waves become sensitive to the mantle.

We acknowledge that there are physical effects that are not accounted for in this study. For example, finite frequency effects can introduce some theoretical bias into our results such as apparent anisotropy in an isotropic heterogeneous structure (Lin & Ritzwoller, 2011) at longer periods. In addition, strong coupling between Rayleigh and Love waves will cause polarization anomalies that are not accurately accounted for by the tomography methods we apply (eikonal tomography), particularly if the quasi-Rayleigh and quasi-Love waves are not well separated. Nevertheles, attributing all of the unexpected signals to measurement errors, noise, or theoretical bias is implausible, particularly given the systematics that result in the observations. This includes the comparisons between fast axes and the countervailing amplitude trends of Rayleigh

and Love wave components, which we attribute to Rayleigh-Love coupling. Further research about these topics would be worthwhile but is beyond the scope of this paper.

Although earthquake data have been used in many observational studies of azimuthal anisotropy and in some cases in combination with ambient noise, we focus on the interpretation of ambient noise data alone for the following reasons. First, although we find that earthquake data also show strong anisotropy for all four-signals at long periods, especially the unexpected anisotropy, in some regions the anisotropy inferred from earthquake data differs from that based on ambient noise whereas in some regions they are very similar. We think a likely reason for this discrepancy is the finite-frequency effects. Second, the azimuthal coverage from earthquakes is limited. Third, we inspected the waveforms from earthquake data and these waveforms are often very complex. These factors present challenges to observe azimuthal anisotropy reliably from earthquake data, especially for the 4ψ components.

Observations of Rayleigh wave 2ψ anisotropy have been the primary data used to infer information about anisotropy from surface waves. Observations of Love wave 2ψ and 4ψ anisotropy as well as Rayleigh wave 4ψ provide new information to improve the inference of the elastic tensor in the crust and mantle in the future.

Acknowledgments

The facilities of IRIS Data Services, and specifically the IRIS Data Management Center, were used for access to waveforms, related metadata and/or derived products used in this study. IRIS Data Services are funded through the Seismological Facilities for the Advancement of Geoscience and EarthScope (SAGE) Proposal of the National Science Foundation under Cooperative Agreement EAR-1851048. This study was funded by NSF Grants EAR-1928395 and EAR- 1952209 at the University of Colorado Boulder.

Open Research

The network codes for seismic data used in this study include 5C, 7C, 9C, AK, AT, AV, CN, GM, II, IM, IU, PN, PO, PP, TA, US, XE, XF, XI, XN, XR, XV, XY, Y2, YE, YG, YM, YV, ZE, ZQ. Earthquake Rayleigh wave 2ψ azimuthal anisotropy used in Fig. S8 is available on Zenodo (Liu, et al., 2022, https://doi.org/10.5281/zenodo.7080282). Original seismic waveform

460 data were obtained from the Data Management Center of IRIS (www.iris.edu). ObsPy
461 (Beyreuther et al. 2010) is used in data processing. Some figures were made using Generic
462 Mapping Tools (GMT) version 6 (Wessel, et al., 2019) licensed under LGPL.
463

464 **References**

465 Backus, G. E. (1965). Possible forms of seismic anisotropy of the uppermost mantle under
466 oceans. Journal of Geophysical Research, 70(14), 3429-3439.
467

468 Beyreuther, M., Barsch, R., Krischer, L., Megies, T., Behr, Y., & Wassermann, J. (2010). ObsPy:
469 A Python toolbox for seismology. Seismological Research Letters, 81(3), 530-533.
470

471 Ekström, G. (2011). A global model of Love and Rayleigh surface wave dispersion and
472 anisotropy, 25-250 s. Geophysical Journal International, 187(3), 1668-1686.
473

474 Feng, L., Liu, C., & Ritzwoller, M. H. (2020). Azimuthal anisotropy of the crust and uppermost
475 mantle beneath Alaska. Journal of Geophysical Research: Solid Earth, 125(12), e2020JB020076.
476

477 Forsyth, D. W. (1975). The early structural evolution and anisotropy of the oceanic upper
478 mantle. Geophysical Journal International, 43(1), 103-162.
479

480 Kawakatsu, H. (2016). A new fifth parameter for transverse isotropy. Geophysical Journal
481 International, 204(1), 682-685.
482

Lévěque, J. J., Debayle, E., & Maupin, V. (1998). Anisotropy in the Indian Ocean upper mantle from Rayleigh-and Love-waveform inversion. Geophysical Journal International, 133(3), 529-540.

Levshin, A. L., Ritzwoller, M. H., Barmin, M. P., Villasenor, A., & Padgett, C. A. (2001). New constraints on the arctic crust and uppermost mantle: surface wave group velocities, Pn, and Sn. Physics of the Earth and Planetary Interiors, 123(2-4), 185-204.

Lin, F. C., Ritzwoller, M. H., & Snieder, R. (2009). Eikonal tomography: surface wave tomography by phase front tracking across a regional broad-band seismic array. Geophysical Journal International, 177(3), 1091-1110.

Lin, F. C., & Ritzwoller, M. H. (2011). Apparent anisotropy in inhomogeneous isotropic media. Geophysical Journal International, 186(3), 1205-1219.

Lin, F. C., Ritzwoller, M. H., Yang, Y., Moschetti, M. P., & Fouch, M. J. (2011). Complex and variable crustal and uppermost mantle seismic anisotropy in the western United States. Nature Geoscience, 4(1), 55-61.

Liu, C., Zhang, S., Sheehan, A. F., & Ritzwoller, M. H. (2022). Surface wave isotropic and azimuthally anisotropic dispersion across Alaska and the Alaska-Aleutian subduction zone. Journal of Geophysical Research: Solid Earth, 127(11), e2022JB024885.

506 Liu, C., Zhang, S., Sheehan, A. F., & Ritzwoller, M. H. (2022). Surface Wave Isotropic and
507 Azimuthally Anisotropic Dispersion across Alaska and the Alaska-Aleutian Subduction Zone
508 [Dataset]. Zenodo. https://doi.org/10.5281/zenodo.7080282
509
510 Liu, C., Sheehan, A. F., & Ritzwoller, M. H. (2024). Seismic azimuthal anisotropy beneath the
511 Alaska subduction zone. Geophysical Research Letters, 51, e2024GL109758.
512
513 Liu, C., & Ritzwoller, M. H. (2024). Seismic anisotropy and deep crustal deformation across
514 Alaska. Journal of Geophysical Research: Solid Earth, 129(5), e2023JB028525.
515
516 Liu, X., & Ritzwoller, M. H. (2025). The effect of Rayleigh–Love coupling in an anisotropic
517 medium. Geophysical Journal International, 241(2), 1204-1225.
518
519 Liu, Z., Liang, C., Cao, F., Fan, X., & Chen, C. (2025). Mechanisms for layered anisotropy and
520 anomalous magmatism of Alaska subduction system revealed by ambient noise tomography and
521 the wave gradiometry method. Journal of Geophysical Research: Solid Earth, 130(1),
522 e2024JB029105.
523
524 Montagner, J. P., & Nataf, H. C. (1986). A simple method for inverting the azimuthal anisotropy
525 of surface waves. Journal of Geophysical Research: Solid Earth, 91(B1), 511-520.
526
527 Montagner, J. P., & Jobert, N. (1988). Vectorial tomography—ii. Application to the Indian
528 Ocean. Geophysical Journal International, 94(2), 309-344.
529

Montagner, J. P., & Tanimoto, T. (1990). Global anisotropy in the upper mantle inferred from the regionalization of phase velocities. Journal of Geophysical Research: Solid Earth, 95(B4), 4797-4819.

Mauerberger, A., Maupin, V., Gudmundsson, Ó., & Tilmann, F. (2021). Anomalous azimuthal variations with 360° periodicity of Rayleigh phase velocities observed in Scandinavia. Geophysical Journal International, 224(3), 1684-1704.

Nishimura, C. E., & Forsyth, D. W. (1988). Rayleigh wave phase velocities in the Pacific with implications for azimuthal anisotropy and lateral heterogeneities. Geophysical Journal International, 94(3), 479-501.

Russell, J. B., Gaherty, J. B., Lin, P. Y. P., Lizarralde, D., Collins, J. A., Hirth, G., & Evans, R. L. (2019). High-resolution constraints on Pacific upper mantle petrofabric inferred from surface-wave anisotropy. Journal of Geophysical Research: Solid Earth, 124(1), 631-657.

Smith, M. L., & Dahlen, F. A. (1973). The azimuthal dependence of Love and Rayleigh wave propagation in a slightly anisotropic medium. Journal of Geophysical Research, 78(17), 3321-3333.

Schulte-Pelkum, V., Caine, J. S., Jones III, J. V., & Becker, T. W. (2020). Imaging the tectonic grain of the northern Cordillera orogen using Transportable Array receiver functions. Seismological Society of America, 91(6), 3086-3105.

554 Schulte-Pelkum, V., Bender, A., & Ruppert, N. A. (2023). Seismicity and anisotropic imaging
555 reveal an active detachment beneath the northern Alaska range foothills. Authorea Preprints.
556
557 Tanimoto, T., & Anderson, D. L. (1985). Lateral heterogeneity and azimuthal anisotropy of the
558 upper mantle: Love and Rayleigh waves 100–250 s. Journal of Geophysical Research: Solid
559 Earth, 90(B2), 1842-1858.
560
561 Trampert, J., & Woodhouse, J. H. (2003). Global anisotropic phase velocity maps for
562 fundamental mode surface waves between 40 and 150 s. Geophysical Journal International,
563 154(1), 154-165.
564
565 Visser, K., Trampert, J., & Kennett, B. L. N. (2008). Global anisotropic phase velocity maps for
566 higher mode Love and Rayleigh waves. Geophysical Journal International, 172(3), 1016-1032.
567
568 Wang, Y., & Tape, C. (2014). Seismic velocity structure and anisotropy of the Alaska subduction
569 zone based on surface wave tomography. Journal of Geophysical Research: Solid Earth, 119(12),
570 8845-8865.
571
572 Wessel, P., Luis, J. F., Uieda, L., Scharroo, R., Wobbe, F., Smith, W. H. F., & Tian, D. (2019).
573 The Generic Mapping Tools version 6. Geochemistry, Geophysics, Geosystems, 20, 5556–5564.
574 https://doi.org/10.1029/2019GC008515
575

576 Xie, J., Ritzwoller, M. H., Brownlee, S. J., & Hacker, B. R. (2015). Inferring the oriented elastic
577 tensor from surface wave observations: preliminary application across the western United States.
578 Geophysical Journal International, 201(2), 996-1021.
579
580 Xie, J., Ritzwoller, M. H., Shen, W., & Wang, W. (2017). Crustal anisotropy across eastern Tibet
581 and surroundings modeled as a depth-dependent tilted hexagonally symmetric medium.
582 Geophysical Journal International, 209(1), 466-491.
583
584 Yao, H., van Der Hilst, R. D., & Montagner, J. P. (2010). Heterogeneity and anisotropy of the
585 lithosphere of SE Tibet from surface wave array tomography. Journal of Geophysical Research:
586 Solid Earth, 115(B12).
587
588 Yuan, H., & Romanowicz, B. (2010). Lithospheric layering in the North American craton.
589 Nature, 466(7310), 1063-1068.
590
591 Yuan, K., & Beghein, C. (2014). Three-dimensional variations in Love and Rayleigh wave
592 azimuthal anisotropy for the upper 800 km of the mantle. Journal of Geophysical Research: Solid
593 Earth, 119(4), 3232-3255.
594
595 Zeng, Q., Lin, F. C., & Tsai, V. C. (2024). Spurious Rayleigh-wave apparent anisotropy near
596 major structural boundaries: a numerical and theoretical investigation. Geophysical Journal
597 International, 239(2), 901-913.
598

599 Zhu, H., & Tromp, J. (2013). Mapping tectonic deformation in the crust and upper mantle
600 beneath Europe and the North Atlantic Ocean. Science, 341(6148), 871-875.
601
602 Zhu, H., Yang, J., & Li, X. (2020). Azimuthal anisotropy of the North American upper mantle
603 based on full waveform inversion. Journal of Geophysical Research: Solid Earth, 125(2),
604 e2019JB018432.
605
606 Zhang, S., Feng, L., & Ritzwoller, M. H. (2020). Three-station interferometry and tomography:
607 coda versus direct waves. Geophysical Journal International, 221(1), 521-541.
608
609 Zhang, S., Wang, H., Wu, M., & Ritzwoller, M. H. (2021). Isotropic and azimuthally anisotropic
610 Rayleigh wave dispersion across the Juan de Fuca and Gorda plates and US Cascadia from
611 earthquake data and ambient noise two-and three-station interferometry. Geophysical Journal
612 International, 226(2), 862-883.